Neuronal synchrony and the relation between the BOLD response and the local field potential

Dora Hermes[1,2,3],*

Mai Nguyen[4],

Jonathan Winawer[1]*

[1] *Department of Psychology, New York University, New York, New York, USA*

[2] *Brain Center Rudolf Magnus, Dept Neurology & Neurosurgery, University Medical Center Utrecht, The Netherlands*

[3] *Department of Psychology, Stanford University, Stanford, California, USA*

[4] *Department of Psychology, Princeton University, Princeton, New Jersey, USA*

* Corresponding authors: dorahermes@gmail.com, jonathan.winawer@nyu.edu Phone: 212 998-7922, Fax: 212 995-4349

Table of Contents

SUMMARY **1**

1. INTRODUCTION **2**

2. RESULTS **3**

2.1 RELATIONSHIP BETWEEN LFP AND BOLD: ANALYTIC FRAMEWORK 4

2.2 RELATIONSHIP BETWEEN LFP AND BOLD: SIMULATED EXPERIMENTS 6

2.2.1 Simulations of BOLD and LFP responses from neuronal population activity *6*

2.2.2 Broadband and alpha LFP, but not gamma LFP, correlate with BOLD *10*

2.3 RELATIONSHIP BETWEEN ECOG AND FMRI: DATA 11

2.4 DATA MODEL COMPARISON 12

2.4.1 Predicting the BOLD amplitude from features of the LFP *12*

2.4.2 Correlation between BOLD and LFP across all frequencies *16*

3. DISCUSSION **17**

3.1 CHANGES IN BROADBAND POWER PREDICT BOLD 18

3.2 CHANGES IN NARROWBAND GAMMA POWER DO NOT PREDICT BOLD 19

3.3 NEURONAL SYNCHRONY AND THE BOLD SIGNAL 20

3.4 DC OFFSETS AND THE BOLD SIGNAL 21

3.5 A SINGLE MODELING FRAMEWORK ACCOUNTS FOR PATTERNS OF LFP/BOLD CORRELATIONS ACROSS SITES 22

3.6 THE ROLE OF A SIMPLE MODEL IN UNDERSTANDING THE RELATION BETWEEN BOLD AND LFP 22

3.7 REPRODUCIBLE COMPUTATIONS 23

3.8 CONCLUSIONS 23

4. EXPERIMENTAL PROCEDURES **24**

4.1 SIMULATED NEURONAL TIME SERIES 24

4.2 STIMULI AND TASK 24

4.3 ECOG PROCEDURE 24

4.4 FMRI PROCEDURE 24

4.5 PREDICTING FMRI SIGNALS DIRECTLY FROM ECOG MODELS 25

ACKNOWLEDGEMENTS **25**

REFERENCES **26**

Summary

The most widespread measures of human brain activity are the blood oxygen level dependent (BOLD) signal and surface field potential. These measures provide complementary information about human brain activity. To develop an understanding of how to interpret these signals, we developed a model of (a) neuronal population responses, and (b) transformations from neuronal responses into the fMRI BOLD signal and electrocorticographic (ECoG) field potential. Rather than seeking a transformation between signals directly, this approach interprets each measure with respect to the underlying neuronal population responses. Our model accounts for the relationship between BOLD and ECoG data from human visual cortex (V1-V3), matching in three ways: BOLD and ECoG broadband were positively correlated, BOLD and alpha (8-13Hz) were negatively correlated, and BOLD and narrowband gamma (30-80Hz) did not correlate. We infer that features of the field potential that are uncorrelated with BOLD arise largely from changes in synchrony, rather than level, of neuronal activity.

1. Introduction

Most measurements of activity in the living human brain arise from the responses of large populations of neurons, spanning the millimeter scale of functional magnetic resonance imaging (fMRI) and electrocorticography (ECoG) to the centimeter scale of electro- and magneto-encephalography (EEG and MEG). Integrating results across methods is challenging because the signals measured by these instruments differ in spatial and temporal sensitivity, and in the manner by which they combine the underlying neuronal population activity (Buzsaki et al., 2012; Hämäläinen et al., 1993; Logothetis and Wandell, 2004). Differences in scale can be partially bridged by bringing the measurements into register. For example, EEG and MEG sensor data can be projected to cortical sources subject to constraints from simultaneously recorded fMRI data (George et al., 1995) or from independent fMRI localizers (Cottereau et al., 2015), and ECoG electrodes can be aligned to a high resolution anatomical MRI image (Hermes et al., 2010) and compared to the local fMRI signal.

Yet even when electrophysiological and fMRI data are spatially registered, striking differences in the sensitivity to stimulus and task are often observed, indicating differences in how neuronal responses contribute to the measured physiological signals. For example, the fMRI BOLD signal and EEG evoked potentials differ in which brain areas are most sensitive to visual motion (area MT+ with fMRI (Huk et al., 2001) versus V1 and V3A with EEG (Ales and Norcia, 2009)). Within the same visual area, fMRI and source-localized EEG evoked potentials can show different effects of task in similar experimental paradigms, such as the effect of spatial attention on the contrast response function (additive in fMRI (Pestilli et al., 2011), multiplicative in EEG (Itthipuripat et al., 2014)). Even when the spatial scale of the two signals is approximately matched at acquisition, such as ECoG electrodes and fMRI voxels (both at ~2 mm), systematically different patterns of responses can be obtained, such as compressive spatial summation in fMRI versus nearly linear summation in ECoG steady state potentials (but not ECoG broadband signals) (Winawer et al., 2013). Such fundamental functional differences cannot be explained by numerical measurement-to-measurement transformations. Rather, these differences must reflect the fact that the measurements are based on different aspects of the neural population response. To explain the differences in measurement modalities requires a computational framework that derives each of these signals from the neuronal responses.

One approach toward developing such a framework has been to measure the BOLD signal and electrophysiological signals simultaneously, or separately but using the same stimulus and task conditions, and to ask how features of the electrophysiological response compare to the BOLD signal. This approach has revealed important patterns, yet after several decades of careful study, some apparent discrepancies remain. A number of studies comparing band-limited power in field potential recordings to the BOLD signal have shown that increases in power between 30 and 100 Hz (gamma band) are more highly correlated with BOLD amplitude than power changes in other bands (Goense and Logothetis, 2008; Lachaux et al., 2007; Logothetis et al., 2001; Mukamel et al., 2005; Niessing et al., 2005; Shmuel et al., 2006). Yet power changes in this band do not fully account for the BOLD signal: very large power changes can occur in the gamma band without a measurable BOLD signal change (Muthukumaraswamy and Singh, 2009; Swettenham et al., 2013), and power changes in lower frequency bands can be correlated with the BOLD signal independently of power changes in the gamma band (Harvey et al., 2013; Maier et al., 2008; Scheeringa et al., 2011; Scheeringa et al., 2016). It therefore cannot be the case that field potential power in the gamma band is a general predictor of BOLD, even if the two measures are often correlated. Another source of disagreement is that within the gamma band, some reports claim that BOLD is best predicted by synchronous (narrowband) signals (Niessing et al., 2005), and others claim that BOLD is best predicted by asynchronous (broadband) neural signals (Winawer et al., 2013). Moreover, in some

cases, it has been reported that no feature of the local field potential predicts the intrinsic optical imaging signal (closely related to BOLD) as accurately as multiunit spiking activity (Lima et al., 2014). Consistent with this claim, a comparison of both motion and contrast response functions measured with single units and with BOLD suggested a tight coupling between BOLD and single unit responses (Heeger et al., 2000; Heeger and Ress, 2002; Rees et al., 2000). To our knowledge, there is currently no single model linking the electrophysiological and BOLD signals that accounts for the wide range of empirical results.

The numerous studies correlating features of electrophysiological signals with BOLD provide constraints in interpreting the relationship between the two types of signals, yet the approach has not led to a general, computational solution. We argue that one reason that correlation studies have not led to computational solutions is that any particular feature of the field potential could be caused by many possible neuronal population responses. For example, a flat field potential (minimal signal) could arise because there is little activity in the local neuronal population, or it could arise from a pair of neuronal sub-populations responding vigorously but in counterphase, resulting in cancellation in the field potential. The same field potential in the two situations would be accompanied by different levels of metabolic demand and presumably different levels of BOLD signal. Similarly, any particular BOLD measurement could be due to many different patterns of neural activity. For example, stimulation of a neuronal population that inhibits local spiking can cause an elevation in the BOLD signal (Mathiesen et al., 1998), as can stimulation of an excitatory population that increases the local spike rate (Lee et al., 2010). In short, there can be no single transfer function that predicts the BOLD signal from the field potential, because the field potential does not *cause* the BOLD signal; rather, the neuronal activity gives rise to both the field potential and the BOLD signal.

We propose that many of the different claims pertaining to the relationship between BOLD amplitude and features of the field potential can be accounted for by a modeling framework in which BOLD and field potential measurements are predicted from simulated neuronal population activity, rather than by predicting the BOLD signal directly from the field potential (Figure 1a versus 1b). In this paper, we model fMRI and ECoG responses in two stages, one stage in which we simulate activity in a population of neurons, and a second stage in which we model the transformation from the population activity to the instrument measures. We then analyze the simulated instrument measures in precisely the same manner in which we analyze data obtained from fMRI and ECoG measurement of visual cortex. By design, the model employs a minimal set of principles governing how the instruments pool neural activity, rather than a biophysically detailed description of neural and hemodynamic events, enabling us to ask whether this minimal set of principles, together with simulated neuronal population activity, can simultaneously account for the empirical BOLD and ECoG measurements.

2. Results

We first present an analytic framework to capture basic principles of how the BOLD signal and the field potential pool neuronal signals across a population. Second, we apply this framework to predict ECoG and BOLD responses, and quantify how the simulated ECoG data are related to the simulated BOLD data. Third, we present results from ECoG and fMRI experiments in human V1, V2 and V3 and assess how well the predictions from the simulation can account for the relationship between ECoG and BOLD observed in the data.

2.1 Relationship between LFP and BOLD: analytic framework

The fMRI BOLD signal and the local field potential (LFP) measure neuronal population activity in a fundamentally different manner. The goal of this analytic framework is to capture these differences in simple mathematical expressions, and from these expressions derive the relationship between the two instrument measurements. We purposely omit a large number of biophysical details such as cell types, neuronal compartments, the dynamics of blood flow, and so forth, both for tractability and in order to emphasize the basic principles of how different measures integrate neuronal activity. In the sections that follow, we then show that, when coupled to simulated neural responses, the model can account for many important patterns observed in fMRI and ECoG data from human visual cortex.

For this analytic framework, we consider how a population of n neurons responds to a stimulus or task during a brief epoch (time 0 to T), assumed to be on the order of a second. Each neuron will produce a time varying dendritic current, denoted as $I_i(t)$ for the ith neuron, resulting from the trans-membrane potential. We would like to know how these currents, $I_i(t)$, relate to the fMRI BOLD signal and to the LFP signal measured by an ECoG electrode.

We assume that the LFP arises primarily from dendritic membrane currents (Buzsaki et al., 2012). We ignore output spikes[1]. For the ith neuron, the contribution to the LFP is then $\alpha_i \times I_i(t)$. The constant α_i depends on the distance and orientation of the neuron with respect to the electrode, as well as the electrode's impedance. For simplicity, we assume that each neuron is equidistant from the electrode and has the same orientation, like pyramidal neurons perpendicular to the cortical surface, and therefore its contribution to the electrode measurement is scaled by the same constant, α. Because currents add, the LFP time series will sum the contribution from each neuron,

$$LFP(t) = \alpha \cdot \sum_{i}^{n} I_i(t) \qquad \text{(Equation 1)}$$

Field potential recordings are usefully summarized as the power (or band-limited power) in the time series (Pesaran, 2008). Here we summarize the LFP response within a short time window as the power in the signal summed over the time window T:

$$LFP\ power = \alpha \cdot \int_0^T \left(\underbrace{\left[\sum_{i}^{n} I_i(t) \right]^2}_{\text{power of sum}} \right) dt \qquad \text{(Equation 2)}$$

Importantly, Equation 2 is a linear/ nonlinear (L/N) computation, since the LFP power is computed by first summing the signals (L), and then computing the power (N).

The BOLD signal pools neural activity in a fundamentally different manner because it depends on metabolic demand (e.g., for reviews, see Logothetis and Wandell, 2004; Raichle and Mintun, 2006). The metabolic demand of each neuron will increase if the cell depolarizes (excitation) or hyperpolarizes (inhibition) (Mathiesen et al., 1998). Hence the metabolic demand of a neuron is a *nonlinear* function of its membrane potential: either a positive or negative change in voltage relative to resting potential causes a current, thereby resulting in a positive metabolic demand.

[1] Although spikes can influence the LFP (Zanos, T.P., Mineault, P.J., and Pack, C.C. (2011). Removal of spurious correlations between spikes and local field potentials. J Neurophysiol 105, 474-486.), it is generally thought that the influence is smaller than synaptic and dendritic currents (Buzsaki, G., Anastassiou, C.A., and Koch, C. (2012). The origin of extracellular fields and currents--EEG, ECoG, LFP and spikes. Nat Rev Neurosci 13, 407-420.), and including spikes would not change the logic of our arguments.

There are many possible nonlinear functions one could assume to summarize the metabolic demand from the dendritic time series, such as the rectified signal (absolute value) or the power (squared signal). For tractability, we assume the metabolic demand of the *i*th neuron is proportional to the power in the time varying trans-membrane current, integrated over time: $\beta_i \times (POWER(I_i(t))$, or $\beta_i \times \int_0^T (I_i(t)^2)dt$, with β_i a scaling constant for the *i*th neuron. (Similar results were obtained if used the absolute value rather than the power). For the entire population of *n* neurons, we then assume the BOLD signal will sum the metabolic demand of each neuron. For simplicity we use the same scaling constant for each neuron:

$$BOLD = \beta \cdot \sum_i^n \left(\int_0^T (I_i(t)^2)dt \right) \qquad \text{(Equation 3)}$$

sum of power

Importantly, Equation 3 is a nonlinear / linear (N/L) computation, since the power is computed first (N) and then the signals are summed (L), opposite to the order of operations for the LFP in Equation 3 (Figure 1) (Personal communication from David J Heeger). In other words, we approximate the BOLD signal as the sum of the power, and LFP as the power of the sum, of the separate neuronal time series. The difference in the order of operations can have a profound effect on the predicted signals, as in the simple example with 2 neurons depicted in Figure 1c and 1d. The BOLD signal pooled over the two neurons is the same whether the time series from the two neurons are in phase or out of phase, whereas the LFP power is large when the time series are in phase and small when they are out of phase.

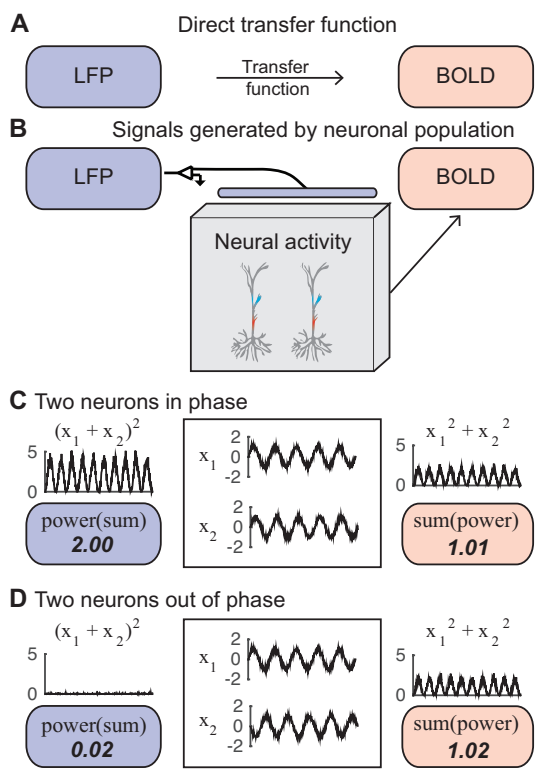

Figure 1. Pooling with different orders of operations can have a large effect on measured brain signals. A) The approach to directly correlate LFP and BOLD data. **B)** Current approach to infer the LFP and BOLD from activity in a neuronal population. **C)** In this illustration the membrane potential of two neurons (x_1 and x_2) has the shape of a sinusoid with noise, and the sinusoid is in phase between the two neurons. In the simulated electrode measurement the signals are summed and the power is calculated (POWER(SUM) = 2.00). In the simulated measurement of metabolic demand, the power of each of these neurons is first calculated, and then summed across the neurons (SUM(POWER) = 1.01). Here, the POWER(SUM) > SUM(POWER). **D)** In this illustration the membrane potential of two neurons (x_1 and x_2) is the same as in panel C except that the two time series are in counterphase. Here, opposite from C), POWER(SUM) < SUM(POWER).

These approximations allow us to make predictions about the relation between LFP and BOLD. By theorem, we know that the power of the sum of several time series is exactly equal to the sum of the power of each time series plus the sum of the cross-power between the different time series (Equation 4):

$$\int_0^T \left(\left[\sum_i^n X_i(t) \right]^2 \right) dt \;=\; \sum_i^n \left(\int_0^T (X_i(t)^2) dt \right) + \sum_{i \neq j}^n \left(\int_0^T \left(X_i(t) \cdot X_j(t) \right) dt \right) \qquad \text{(Equation 4)}$$

Power of sum Sum of power Sum of cross-power

Applying this theorem to Equations 2 and 3 shows the relationship between our model of BOLD and LFP power:

$$LFP\ power = {}^{\alpha}/_{\beta} \cdot BOLD \;+\; \alpha \cdot \sum_{i \neq j}^n \left(\int_0^T \left(I_i(t) \cdot I_j(t) \right) dt \right) \qquad \text{(Equation 5)}$$

We can now see that the LFP power depends on two quantities, one of which is related to the BOLD signal, and one of which is unrelated to the BOLD signal (Equation 5). The first term summarizes the total level of neural activity (summed across neurons), and the second term summarizes the relationship between neural time series (the cross-power, similar to covariance). If and when the second term tends to be large compared to the first, then the LFP power will not be closely related to the BOLD signal.

One cannot deduce from first principles whether the first term in Equation 4 (summed power) or the second term (summed cross-power) will dominate. However, he number of elements contributing to the two terms is quite different: For n neurons, the first term grows with n (the power in each neuron's time series), whereas the second term grows with n^2 (all the pairwise cross-powers). Hence if there is any appreciable covariance, then the LFP power will be dominated by the second term, and the correlation with BOLD will be weak (except in cases where the cross-power and power are highly correlated).

2.2 Relationship between LFP and BOLD: simulated experiments

We next used the framework above to compute the BOLD and LFP signals as a function of simulated neuronal population activity.

2.2.1 Simulations of BOLD and LFP responses from neuronal population activity

Cortical neurons receive a large number of inputs from diverse cell types. We simulated three inputs to each neuron (Figure 2a). Input 1 approximated Poisson-like spike arrivals (C^1, 'Broadband'). Input 2 was a high frequency oscillation, peaked between 40 and 60 Hz, coordinated between neurons (C^2, 'Gamma'). Input 3 was a low frequency inhibitory signal, 8-12 Hz (C^3, 'Alpha'). For each simulated neuron i, the total input C on each trial is the sum of these three signals (Figure 2b):

$$C_i(t) = \; C_i^1(t) \;+\; C_i^2(t) + \; C_i^3(t) \qquad \text{(Equation 6)}$$

We then passed the summed input in each neuron through a leaky integrator to produce the time-varying dendritic current for that neuron (I_i, Figure 2c):

$$\tau \cdot {}^{dI_i}/_{dt} = -I_i(t) + C_i(t) \qquad \text{(Equation 7)}$$

The membrane time constant, τ reflects the time dependence of the trans-membrane current (Koch et al., 1996; Miller et al., 2009a). In total, we modeled a population of 200 neurons, each of which produced a one-second time series on each trial. To match the design of our ECoG experiments, a simulated experiment consisted of 240 1-s trials (30 repeats of 8 conditions). Below we explain (1) how the time series was generated for each of the three types of inputs, and (2) how the input levels varied for the 8 conditions.

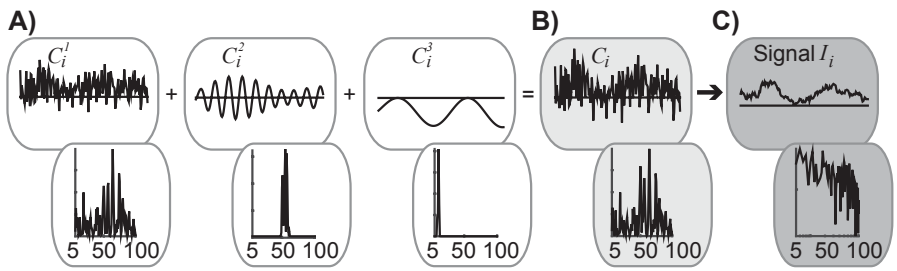

Figure 2. Simulated model inputs. A) Three different inputs to each neuron were simulated: a broadband, random input with a small positive offset (C_i^1), an oscillatory input with a time-scale of 40-60Hz (C_i^2), and a negative input with a time-scale of 10 Hz (C_i^3). The bottom panel shows the power spectra for each of the three inputs. **B)** The three inputs were summed in each neuron to produce the total input to the neuron (C_i). **C)** The total input was passed through a leaky integrator to produce the dendritic dipole current (I_i).

Broadband input (C^1). Input C^1 was Gaussian white noise with a small positive bias. The Gaussian white noise approximates Poisson distributed spike arrivals, each of which produces a small positive or negative conductance change, corresponding to excitatory or inhibitory post-synaptic potentials. The small positive bias reflects the assumption of more excitatory than inhibitory synaptic currents, causing a net depolarization. Gaussian white noise was used rather than Poisson distributed synaptic inputs for computational efficiency, but the pattern of results is similar for Poisson or Gaussian distributions. With C^1, we simulated high versus low rates of spike arrivals across simulation trials by using large versus small standard deviations of the Gaussian distributions. For all simulations, the coherence was zero between the 200 neurons in the population, meaning the time series in each neuron was independent except for chance correlations. This white noise input, after passing through leaky integration, results in an output whose power spectral density declines with temporal frequency. When the level of this input increases (higher standard deviation of the noise distribution), the result is a broadband elevation in power (Miller et al., 2009a) (Figure 3, left panel), an effect that can be observed in the local field potential (Henrie and Shapley, 2005) as well as intracellular membrane potentials of single neurons in awake macaque (Tan et al., 2014).

Gamma input (C^2). Input C^2 consisted of band pass noise (40-60 Hz), with fixed amplitude on all trials, and with coherence across neurons that varied between trials. This input approximates the signals giving rise to narrowband gamma oscillations. Across different conditions, we varied the coherence between neurons of C^2 rather than the amplitude for individual neurons, which was fixed. The motivation for this comes from empirical observations that large gamma oscillations in the LFP tend to reflect increased coherence between neurons (Hasenstaub et al., 2005; Jia et al., 2013a). This is opposite to the broadband input (C^1), for which we varied the amplitude in individual neurons across trials, rather than the synchrony between neurons. Narrowband gamma oscillations with a peak between 30 and 80 Hz can be observed in the local field potential (Gray et al., 1989; Gray and Singer, 1989), as well as in the membrane potential of individual pyramidal neurons (Perrenoud et al., 2016). When we increase the coherence of C^2 in our simulations, the result is an increase in the amplitude of the LFP in the gamma band (Figure 3, middle panel), much like narrowband gamma signals observed in microelectrode recordings (Burns et al., 2011) and human ECoG (Hermes et al., 2015b).

Alpha input (C^3). The alpha input consisted of inhibitory oscillations at approximately 10 Hz, with fixed coherence between neurons, and varying amplitude across trials. The oscillations were inhibitory, i.e. the mean was below the resting potential (compare C^3 versus C^1 and C^2 in Figure 2a). Because C^3 was inhibitory, it results in hyperpolarization (or less depolarization), opposite the effect of C^1, which resulted in depolarization. This input approximates the signals giving rise to

alpha oscillations (Figure 3, right panel). Pyramidal neurons in visual cortex have been hypothesized to receive periodic inhibition, with pulses arriving at approximately 10 Hz (Jensen and Mazaheri, 2010; Schalk, 2015). Individual neurons in visual cortex can indeed show subthreshold membrane oscillations at frequencies around 10 Hz (Llinas et al., 1991).

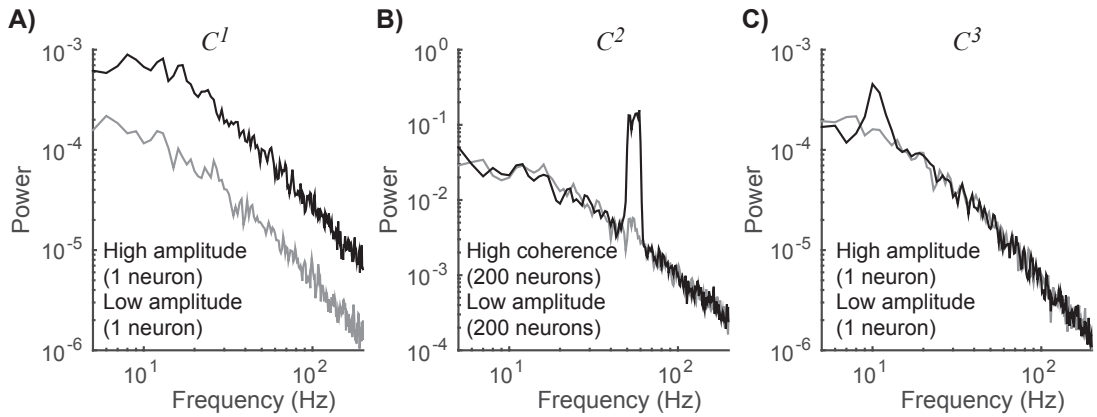

Figure 3. Effect of varying simulated neural inputs on output spectra. Each panel shows the effect of manipulating one of the three neural inputs used in the simulations. For C^1 (broadband), a high amplitude results in a broadband power elevation, evident in individual neurons. For C^2 (gamma), a high coherence results in a narrowband power elevation when the field potential is summed over the population of 200 neurons. For C^3 (alpha), a high amplitude results in a narrowband power elevation in the alpha band, evident in individual neurons. For each spectrum in each plot, 10 simulated trials were run. The plotted spectra are averaged across the 10 trials, and are computed from *I(t)*, the time series after leaky integration of the inputs.

From the neuronal population simulations, we computed the LFP and BOLD signals according to the equations above (section "Relationship between LFP and BOLD: analytic framework"). In brief, the LFP was computed by summing the trans-membrane current across neurons (Equation 1), and the BOLD signal was computed by summing the power across neurons (Equation 3). The BOLD signal was averaged across the 30 trials with the same condition. The LFP time series was transformed to a power spectrum, which was averaged across the 30 repeated trials of the same condition. The average power spectrum was summarized by three components: elevation in broadband power, the power of narrowband gamma oscillations (40-70 Hz), and the power of alpha oscillations (8-12 Hz).

The simulations were structured to approximate the experimental design and the results of our ECoG experiments (Section 2.3). In brief, in the ECoG experiments, there were four grating stimuli of different spatial frequencies, three noise patterns with different power spectra, and one blank stimulus (mean luminance). For each of the 8 stimuli and each of 22 electrodes in V1-V3, we decomposed the measured ECoG responses into the same three components computed from the simulations: broadband, narrowband gamma, and alpha.

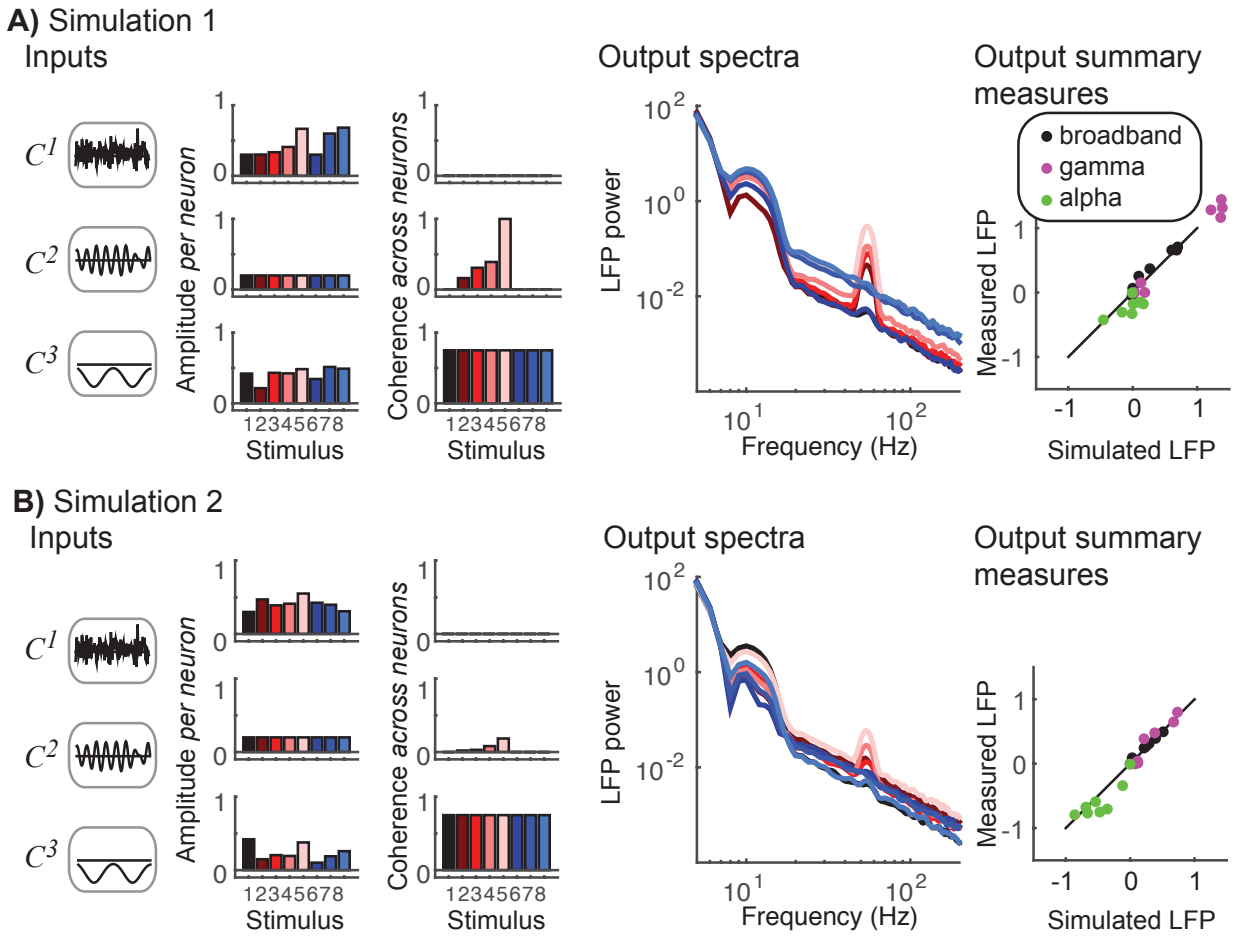

Figure 4. Inputs and outputs of simulations. A) The 8 different stimuli were defined by particular mixtures of the three types of input (C^1, C^2, C^3). The bar plots show the amplitude per neuron and the coherence across neurons for each of the 8 simulated stimuli. The output spectra were computed by summing the time series across the 200 neurons, computing the power spectra on each trial, and averaging the power spectra across 30 repeated trials of the same stimulus. The colors of the traces match the colors of the 8 stimuli in the bar plots. The spectra show broadband changes across all frequencies arising from C^1, a peak around 50 Hz from C^2, and a peak around 10 Hz from C^3. The right panel shows the simulated and measured summary metrics for each of the 8 stimuli: alpha power (green), gamma power (magenta), and broadband (black). The simulated measures are derived from the spectra in the 'Output spectra' panel. The measured metrics are derived from a V1 electrode. The simulated and measured values are close by construction, since the inputs to the simulation were fitted to match the output spectral measurements from this electrode. **B)** Same as A, except that the simulation was matched to a V2 electrode rather than a V1 electrode.

The level of the three inputs, C^1, C^2, and C^3 were determined so that that the simulated summary metrics (broadband, gamma and alpha) matched the measured ECoG summary metrics for each of the 8 conditions for a particular electrode (Figure 4). Importantly, the determination of the input levels did not take into account the measured BOLD responses. Hence the simulations provided a test: if the inputs were chosen to produce outputs that match the measured ECoG responses, does the simulated BOLD signal accurately predict the measured BOLD signal?

We first review two simulations, one matched to ECoG measurements from a V1 electrode, and one matched to ECoG measurements from a V2 electrode. We then summarize the results of 22 simulations corresponding to the 22 electrodes in V1-V3. As with the ECoG experiments, in the simulation each condition was repeated 30 times for 240 trials.

2.2.2 Broadband and alpha LFP, but not gamma LFP, correlate with BOLD

For each of the 8 stimuli in one simulation, we obtained 4 summary responses, a single BOLD amplitude and three LFP measures (broadband, gamma and alpha, Figure 5A). By design, the values of the LFP components (but not BOLD) were close to the values measured in one of the electrodes.

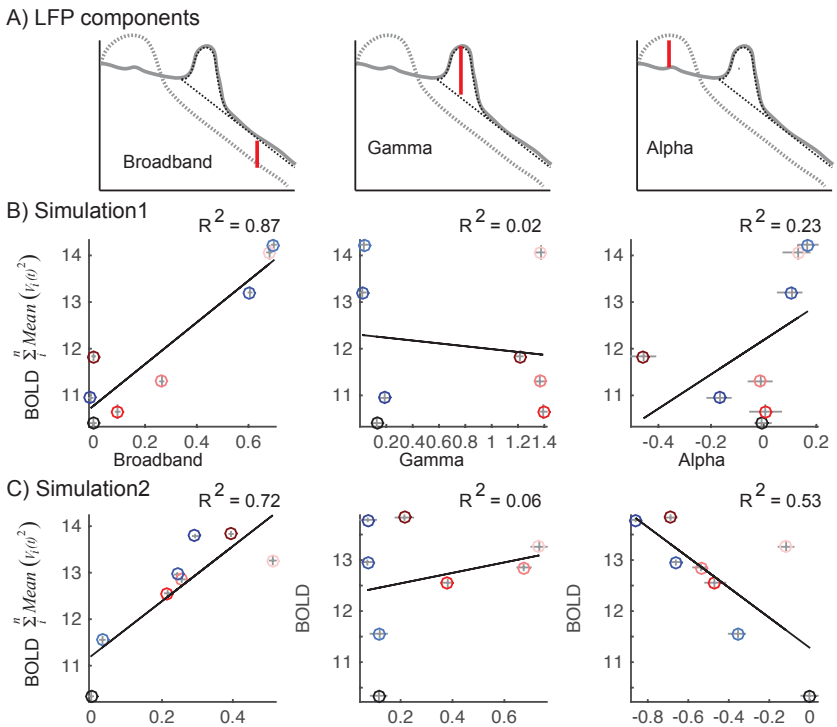

Figure 5. Simulated correlation between BOLD and LFP. A) Schematic to show LFP summary metrics derived from spectra: broadband power elevation, narrowband gamma and alpha. Broadband was calculated by the increase in a $1/f^n$ signal, gamma was calculated by fitting a Gaussian on top of the $1/f^n$ line, and alpha was calculated as the difference from baseline in the alpha-frequency-range. **B)** The levels of C^1, C^2, C^3, and were chosen for each of 8 conditions to approximate the measurements of broadband, gamma, and alpha for 8 different stimuli from a V1 electrode. Red dots indicate that inputs were matched to responses to a grating pattern, blue dots are matched to noise patterns, and black is matched to a blank stimulus. The correlation between broadband and simulated BOLD is high (left), whereas the correlations between gamma and BOLD (middle) and alpha and BOLD (right) are low. Error bars show the 68% confidence interval across bootstraps. **C)** Same as B except that inputs were chosen so that LFP measures matched ECoG data from a V2 electrode. Here, the correlation is high and positive between broadband and BOLD (left), low between gamma and BOLD (middle), and highly negative between alpha and BOLD (right).

For Simulation 1, we observed three patterns (Figure 5B). First, the LFP broadband response correlated highly with BOLD ($R^2 = 0.87$). Second, the power of narrowband gamma oscillations was weakly correlated with BOLD ($R^2 = 0.02$), and third alpha oscillations were weakly correlated with BOLD ($R^2 = 0.23$). In this simulation, the LFP broadband response was the only good correlate of the BOLD signal.

In Simulation 2, the broadband LFP was again a good predictor of BOLD, and gamma power was again a poor predictor (Figure 5C). Unlike Simulation 1, the power of alpha oscillations was strongly negatively correlated with BOLD ($R^2 = 0.53$). The stronger correlation between alpha oscillations and BOLD was not due to a difference in the way the alpha oscillations were simulated, nor to the way BOLD was computed – the simulation algorithm and the analysis code extracting the BOLD and LFP measures were identical. The observations from the two sets of simulations emphasize the fact that the identical mechanism that converts neural activity to BOLD ("neurovascular coupling"), modeled here as power in the time series summed across neurons

(Equation 3), can produce very different correlations between BOLD and features of the LFP. The two sets of simulations differed only in the neural population activity, not in the transfer functions relating neural responses to instrument measurements. The higher correlation between alpha power and BOLD in Simulation 2 versus 1 is due to the fact that the alpha power varied more, and the broadband power varied less, across the 8 stimuli in the simulation.

2.3 Relationship between ECoG and fMRI: Data

The ECoG responses, like the simulated LFP responses, were separated into three components for each stimulus condition in each electrode: a broadband component, a narrowband gamma component, and an alpha component. The separation into the three components was accomplished using the identical analysis code as in the simulated data. An important feature of this data set is that the 3 components of the ECoG response showed different patterns across stimuli (Hermes et al., 2015b): stimuli comprised of noise patterns caused large broadband increases but little to no measureable narrowband gamma response, whereas grating stimuli elicited both broadband increases and narrowband gamma increases. Gratings and noise stimuli resulted in decreases in alpha power compared to baseline (Supplementary Figure S1). Had all three responses been correlated with each other, it would not be possible to infer how each relates separately to the BOLD signal.

We measured BOLD responses in 4 healthy subjects to the same visual stimuli as used in ECoG (subjects are different from the ECoG subjects), and extracted the signal from regions of interest in visual cortex matched to the previously recorded ECoG electrode locations (Supplementary Figure S2 and S3). Combining the ECoG and BOLD data sets enabled us to summarize the data with the same four measures for each stimulus that we used to summarize the simulation: a single BOLD response and three ECoG component responses.

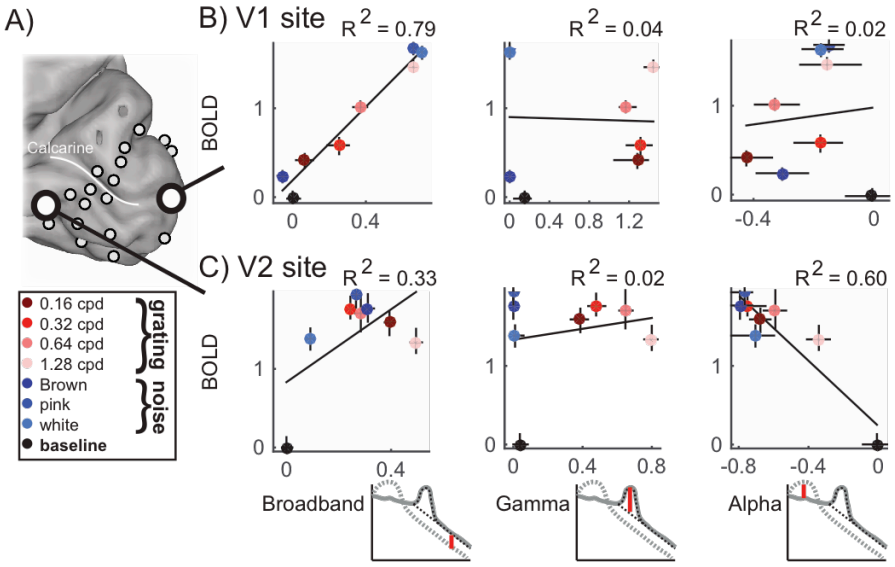

Figure 6. Measured correlation between ECoG and BOLD in V1 and V2/V3. A) The correlation between ECoG and BOLD was calculated for electrodes in V1 and V2/V3. The locations of one sample electrode in V1 and one in V2 are indicated by the enlarged white discs on the cortical surface for subject 1. **B)** In a foveal V1 site, the broadband ECoG amplitude predicted the BOLD signal (left). Error bars show 68% confidence intervals across bootstraps. Narrowband gamma power (center) and alpha power (right) did not predict BOLD. **C)** In a V2 site, the broadband ECoG was weakly correlated with BOLD (left). Narrowband gamma did not predict BOLD (middle). Alpha was negatively correlated with BOLD (right). The schematic spectral plots beneath the scatter plots illustrate the three ECoG components. Scatter plots for all other V1 and V2/V3 sites are shown in Supplementary Figure S5.

We first consider the V1 site that was used to guide the input levels for Simulation 1 (Figure 6B). We emphasize that the BOLD data for this site was not used to guide the simulation (only the ECoG data were used). Three patterns relating the BOLD signal to the ECoG data for this site match Simulation 1. First, the BOLD amplitude for the different stimuli was highly correlated with the broadband response (R^2 = 0.79). Second, the narrowband gamma response was unrelated to BOLD (R^2= 0.04). Third, there was little correlation between BOLD and alpha power (R^2 = 0.02). Hence, as in simulation 1, only broadband power was a good predictor of BOLD amplitude.

A different pattern was found in the V2/V3 data, and this pattern was similar to that observed in Simulation 2. For the V2 site guiding Simulation 2, the correlation between BOLD and broadband was smaller than that found for the V1 channel (R^2 = 0.33), and the correlation between alpha power and BOLD was stronger than for V1, and was negative (R^2 = 0.60). Gamma power did not correlate with BOLD, similar to V1 data and to Simulations 1 and 2.

The differences in the BOLD/ECoG responses in V1 compared to V2/V3 could, in principle, arise either because the neurovascular coupling mechanism differs between the two cortical areas, or because the neural responses for these particular experimental conditions differ in the two areas. While we do not have access to the neurovascular coupling mechanisms nor to the neural response at the individual neuron level, we can compare the measured ECoG responses in the two brain areas. We observe one large difference between V1 and V2/V3, which is that the range of broadband responses elicited by the different stimuli was larger for V1 than for V2/V3: the average broadband increase above baseline was 0.43 log units for V1 and 0.26/0.28 for V2/V3 (Supplementary Figure S4). As shown in Simulations 1 and 2, a difference in the neuronal population responses can result in a different pattern of response between features of the ECoG signal and the BOLD signal.

2.4 Data model comparison

In the example V1 electrode and in Simulation 1, the BOLD signal was well explained by broadband increases (Figure 5B; Figure 6B, left). In the example V2 electrode and in Simulation 2, the BOLD signal was explained by both broadband increases and alpha decreases (Figure 5C, Figure 6C). By explicitly modeling both the population response and the population-to-instrument transformations, we see that a difference in the relation between instrument measures (BOLD and ECoG) can arise from a difference in the population response, without a difference in neurovascular coupling. We now ask (1) whether these effects are consistent across the measured V1 and V2/V3 electrodes, and (2) how a multiple regression model using broadband, gamma and alpha as predictors fits the BOLD response for both data and simulation.

2.4.1 Predicting the BOLD amplitude from features of the LFP

As we argued in the Introduction, we believe there is no single, general transfer function that can predict the BOLD signal from the LFP. Yet a regression model linking the two measures can be a useful way to summarize the results of a particular experiment or simulation, and to compare results between different experiments or simulations. Here, we fit several regression models to each simulation and to the data. The regression models predicted the simulated or measured BOLD response from either a single LFP component (broadband power, gamma power, or alpha power), or from combinations of LFP components (each of the pairwise combinations, and the 3 components together). These models were fit separately for each of the 9 electrodes in V1 and each of the 13 electrodes in V2/V3 (19 electrodes from subject 1; 3 from subject 2), and for the 22 corresponding simulations. Accuracy of each model was assessed by cross-validation. With a cross-validation procedure, there is no advantage in accuracy for models with more free parameters.

Simulations. For the simulations, we expect broadband power to positively predict the BOLD signal and alpha power to negatively predict the BOLD signal, because of the construction of the simulations: broadband and alpha power elevations were achieved by increasing the level of inputs per neuron, rather than coherence; the converse was true for gamma. Nonetheless, solving the regression models can be informative because, as seen in Figure 5, simulations with the identical input types and the identical analysis can lead to different patterns, depending on the mixtures of values simulated. Moreover, the regression analyses of the simulated data provide a baseline against which we can compare the regression analyses of the observed data.

The single parameter models across electrodes in V1 and V2/V3 show the same pattern as the single electrode examples in Figures 5 and 6. For simulations fit to V1 ECoG data, broadband alone was a good predictor of BOLD (average cross validated R^2=0.85 across 9 simulations) while gamma and alpha alone were not (gamma R^2 = 0.15, alpha R^2 = 0.10). For simulations fit to V2/V3 ECoG data, broadband and alpha alone each predicted the BOLD signal with moderate accuracy (broadband R^2 = 0.56, alpha R^2 = 0.59).

For simulations fit to V1 and to V2/V3, the BOLD response was best explained by a regression model combining broadband and alpha (R^2 = 0.95, R^2 = 0.95, Figure 7A and B). The regression coefficients for this model were positive for broadband and negative for alpha. A model that incorporated all three LFP measures – broadband, alpha and gamma – did not explain additional variance for either simulation, confirming our earlier observation that narrowband gamma power was not correlated with BOLD amplitude in simulated data.

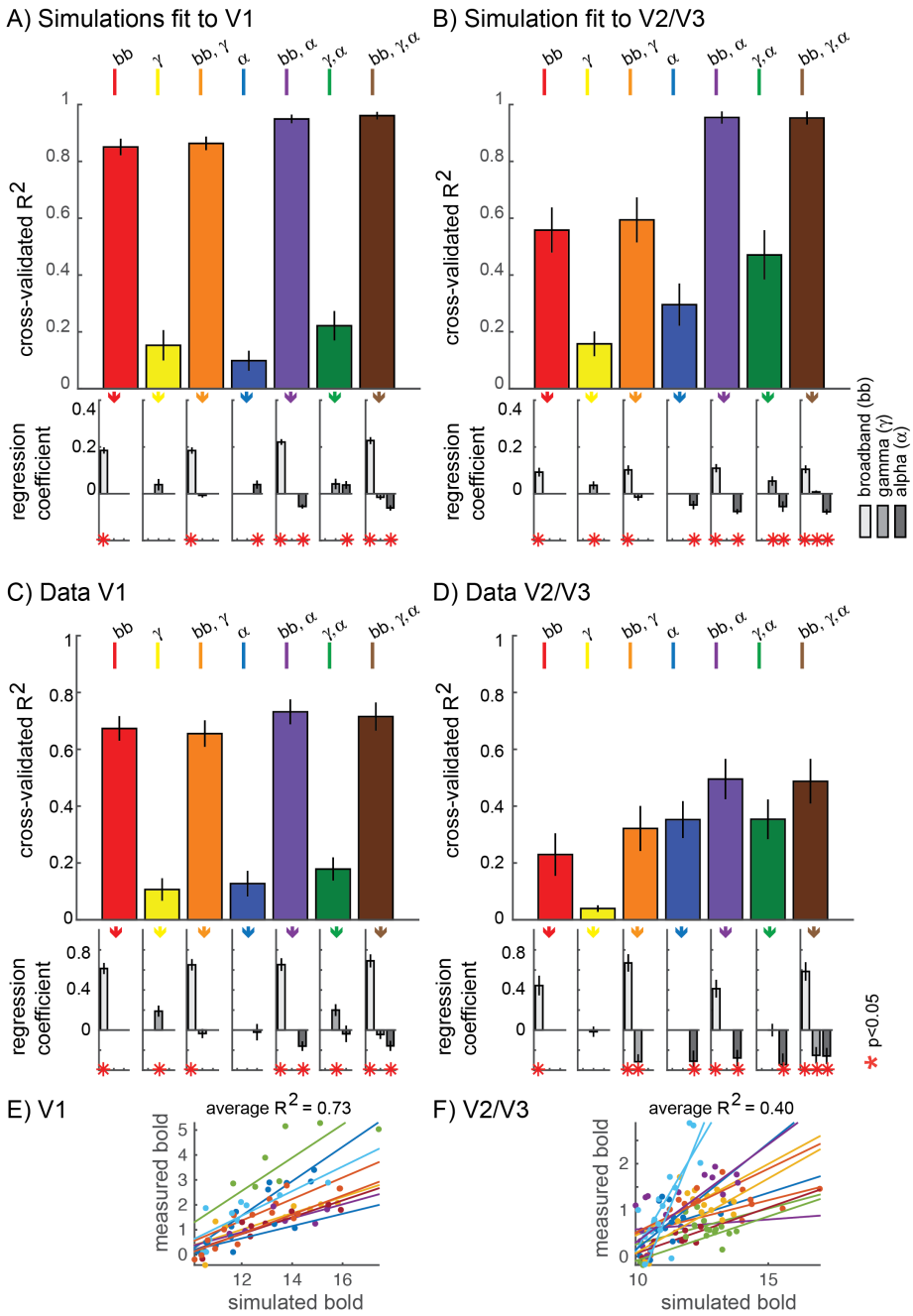

Figure 7. Explained variance in the BOLD fMRI signal in the simulations and in data. A) Variance in the simulated BOLD signal explained by broadband, gamma and alpha changes in the simulated LFP. The colored bars show the R^2 for each of the 7 model types averaged across the 9 simulations fitted to V1 data. Error bars are standard error of the mean across the 9 simulations. The R^2 was cross-validated (split between even and odd stimulus repetitions), to ensure that the R^2 can be compared between models with different numbers of explanatory variables. Bottom: The regression coefficients show whether the broadband, gamma, and alpha signals were positive or negative predictors of the BOLD signal. **B)** Same as A, but for the 13 simulations fitted to V2/V3 ECoG data. **C)** Same as A, but for measured BOLD and ECoG data averaged across the 9 V1 sites. The R^2 was cross-validated (split between subjects for BOLD and stimulus repetitions for ECoG). A red * in the lower plot indicates whether regression coefficients differed significantly from zero by a t-test ($p<0.05$). **D)** Same as C, except for the 13 electrodes in V2/V3. (E) Simulated BOLD (x-axis) versus measured BOLD (y-axis) for the 9 V1 sites. Each color corresponds to one site. The R^2 was computed separately for each of the 9 sites, and then averaged. (F) Same as E, but for V2/V3 sites.

Data. The regression analysis between the measured ECoG and BOLD signal in V1 (Figure 7C) was very similar to the regression analysis in the simulation (Figure 7A). The observed BOLD signal, like the simulated BOLD signal, was best predicted by a combination of broadband and alpha changes (R^2 = 0.73). While narrowband gamma changes were modestly predictive of the BOLD signal across V1 electrodes in a single parameter model (R^2=0.11), adding gamma as a predictor to either the broadband only model (model 2 versus model 1) or to the combined broadband and alpha model (model 7 versus model 5) led to a slight decrease in accuracy, suggesting that any predictive power of gamma alone was probably due to correlation with the other ECoG predictors, rather than a direct relationship to the BOLD signal.

The model fits of the measured BOLD signal in V2/V3 (Figure 7D) were qualitatively similar to the model fits for the V2/V3 data (Figure 7B), though with some quantitative differences. The observed BOLD signal, like the simulated BOLD signal, was best predicted by a combination of broadband and alpha changes (R^2= 0.50) (see also Supplementary Figure S6). As with V1, narrowband gamma in V2/V3 did not explain additional variance in the BOLD signal. Overall, compared to V1, the BOLD signal in V2/V3 was less accurately predicted by the regression models based on the electrophysiological measurements (Figure 7D), and was also less well predicted by the simulated BOLD responses (average R^2 of 35%) (Figure 7F).

Finally, we directly compared the BOLD responses predicted in the simulations with the measured BOLD data. These were in good agreement, with the BOLD data in the simulations accounting for an average of 73% of the variance in the measured data in V1 and 40% in V2 (R^2 averaged across sites) (Figure 7E-F).

Across simulations and data sets, a general pattern emerges. The broadband signal was significantly and positively predictive of BOLD, and alpha power was significantly and negatively predictive of BOLD. Narrowband gamma had no consistent relation with BOLD. While the relationships between broadband and BOLD and alpha power and BOLD were consistent in terms of sign (the former positive, the latter negative), the level was not always the same. As we noted in the example channels shown in Figure 7, the broadband power was more strongly predictive of BOLD in V1, and alpha power was more strongly predictive of BOLD in V2/V3. An examination of responses to the different stimulus types clarifies the difference between V1 and V2/V3 in these data. Specifically, the BOLD response in V2/V3 to noise patterns was under-predicted by the broadband response alone (Supplementary Figure S5). In V2/V3 alpha decreased more for the noise patterns and this alpha decrease accounted for the BOLD change unexplained by broadband (Supplementary Figure S1). This helps to explain why a model that includes broadband and alpha is much more accurate for V2/V3 than a model that includes only broadband. In contrast, for V1 the BOLD response was well predicted by broadband power in most sites, with little systematic prediction failures, and little room for increased model accuracy when adding predictors such as alpha power.

For each of the 22 simulations, the three inputs C^1, C^2, and C^3 defining each of the 8 stimulus conditions were fit to produce the LFP data from the corresponding ECoG electrode. By design, the C^1 (broadband) and C^3 (alpha) inputs were fit to data by varying the *level* per neuron, whereas C^2 was fit to data by varying the coherence across neurons. In principle, for any of the three inputs, the ECoG data could have been fit by varying either the level per neuron or coherence across neurons. For completeness, we tested the 7 alternative models (Supplementary Figure S7). The most accurate model, quantified as the R^2 between the measured BOLD and the simulated BOLD, averaged across the 22 sites, was the simulation type used in the main text, in which C^1 and C^3 varied in the level per neuron and C^2 varied in the coherence across neurons. The simulation in which broadband coherence rather than level modulated broadband power caused a large drop in R^2, The models in which the gamma LFP power was modulated by the coherence rather than the level only caused a small drop in R^2.

2.4.2 Correlation between BOLD and LFP across all frequencies

Simulation. In the previous section, we modeled the BOLD responses as a linear function of three components derived from the LFP. These features - broadband power, narrowband gamma power, and narrowband alpha power - are summary metrics of the power spectrum. We also tested how the power at each frequency in the simulated LFP and in the ECoG data correlated with the BOLD response (simulated and observed). We calculated LFP power for each frequency from 1 to 200 Hz and correlated the power changes from baseline with BOLD changes from baseline (Figure 8). In simulations fit to V1 ECoG data, the LFP correlated well with the BOLD signal across all frequencies except those in the alpha band (8-15 Hz) and below, and those in the gamma band (40-60Hz).

In simulations fit to V2/V3 ECoG data, the pattern was similar, except that the correlation was negative in the alpha band rather than 0, and weaker but still positive in the rest of the spectrum. These patterns match the summary metrics of alpha, gamma, and broadband shown in Figure 7.

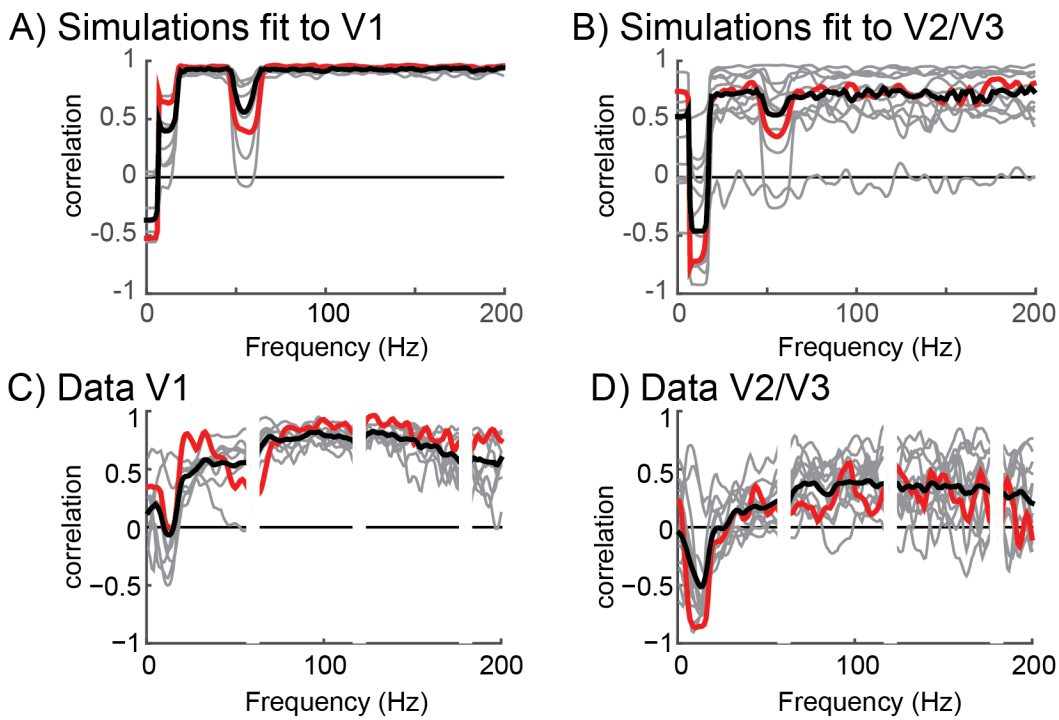

Figure 8. The correlation between BOLD and LFP as a function of frequency. A) The correlation between LFP and BOLD for simulations fit to V1 shows that there is a positive correlation across most frequencies, except those including the alpha and gamma changes. **B)** The correlation between LFP and BOLD for the simulations fit to V2/V3 shows that there is a strong negative correlation around 10 Hz, and a positive correlation across a broad range of frequencies. **C)** In the V1 data there was a positive correlation between ECoG and BOLD for a broad range of frequencies, except those including the alpha changes. Gray lines represent the 9 individual V1 electrodes, the black line is the average, the red line corresponds to the example electrode shown also in Figure 6B, and to the simulation in panel A. **D)** In the V2/V3 data there was a strong negative correlation between ECoG and BOLD in the alpha range around 10 Hz and a positive correlation between ECoG and BOLD for a broad range of frequencies. Gray lines represent the 13 individual V2/V3 electrodes, the black line is the average, the red line corresponds to the example electrode shown also in Figure 6C, and to the simulation plotted in panel B. Note that neither the V1 electrodes nor the V2/V3 electrodes show a peak at the gamma frequency.

Data. The correlation between measured BOLD and ECoG power in V1 was qualitatively similar to that found in simulations. In V1, ECoG responses across all frequencies except the alpha band were positively correlated with the BOLD response (Figure 8C), consistent with the regression analyses

of the summary metrics, showing that broadband ECoG power was the best predictor of the BOLD signal.

The pattern of correlation between ECoG power and BOLD in V2/V3 was similar to that found in V1, although the overall level of correlation was lower. There were positive correlations between ECoG and BOLD extending across most frequencies that were weaker than in V1, and there was a negative correlation for most sites in the alpha band.

There were some differences between V1 sites. For example, in two sites, the correlation across frequencies dipped in the gamma band (30-80Hz), similar to simulated data. These are also the two sites that showed the largest amplitude gamma responses (sites 8 and 9 in Supplementary Figure S5). In other words, when cortical sites showed large gamma signals, these signals were uncorrelated with BOLD. The fact that in 7 V1 sites there was a positive correlation between BOLD and LFP power spanning 30-80 Hz might seem inconsistent with our earlier observation that narrowband gamma power was not predictive of the BOLD signal in V1 sites (Figure 6 and 7). However, in this analysis the narrowband and broadband power are not modeled separately and the positive correlation between power at 30-80 Hz in Figure 8 thus likely suggests that broadband power extends into this band, since broadband changes can extend across all frequencies (Miller et al., 2009a; Winawer et al., 2013). Therefore, if there is little to no narrowband response, we would expect a positive correlation between BOLD and ECoG throughout all frequencies.

There were some site-to-site differences in the correlation between alpha and BOLD. For example, some sites showed a positive correlation with BOLD in the alpha range, and others showed a negative correlation (Figure 8C). These site to site differences depend on the range of responses evoked by stimuli. For example, for electrodes in which stimuli evoked a large of power changes in the alpha band, alpha was more strongly correlated with BOLD. Similarly, for electrodes in which stimuli evoked a large range of broadband responses, broadband was more highly correlated with BOLD (Supplementary Figure S8). This pattern did not hold for narrowband gamma power changes.

3. Discussion

This study investigated the relationship between electrophysiological and BOLD measurements in human visual cortex. Our modeling framework decomposed the signals into two stages, a first stage in which we simulated the neuronal population responses (dendritic time series), and a second stage in which we modeled the transfer of the neuronal time series to the BOLD signal and the field potential. This approach differs from the direct comparison of electrophysiological signals and BOLD. The explicit separation into stages clarified both a similarity and a difference between the BOLD amplitude and the field potential power: the two can be approximated as the same operations on the neuronal population activity, but applied in a different order. Specifically, within a brief window, we modeled the BOLD amplitude as the sum of the power in the neuronal time series, and the field potential as the power of the sum of the neuronal time series. Because the order of operations differs, the two signals differ, and each is blind to particular distinctions in the neuronal activity. For example, the BOLD signal (according to our model) does not distinguish between synchronous and asynchronous neural signals with the same total level of activity. In contrast, the field potential does not distinguish counterphase responses from no response. Even if one knew the exact mechanism of neurovascular coupling and the precise antenna function of an electrode, one still could not predict the relationship between the BOLD signal and the field potential without specifying the neuronal population activity that caused both. Hence the relationship between the two types of signals is not fixed, but rather depends on the structure of the underlying responses of the neuronal population.

Although we do not have access to the complete set of individual neuronal responses in any of our experiments in visual cortex, we approximated the responses by specifying the type of signals common to visual cortex. We therefore limited the space of neuronal population responses by modeling the activity as arising from three types of signals, enabling us to compute the complete set of field potentials and BOLD responses to a variety of conditions. Finally, we compared the simulated patterns of BOLD and field potential responses to the actual responses we observed in data from human subjects. These patterns are discussed and interpreted below.

3.1 Changes in broadband power predict BOLD

Many studies have reported correlations between BOLD and power in the gamma band LFP (30-130 Hz) (review for human studies: (Ojemann et al., 2013)). Yet changes in gamma band power do not reflect a single biological mechanism. For example, several recent studies have emphasized that LFP power changes in the gamma band reflect multiple distinct neural sources, including narrowband oscillations and broadband power shifts, with very different stimulus selectivity and biological origins (Hermes et al., 2015a; Hermes et al., 2015b; Ray and Maunsell, 2011).

Broadband changes have been proposed to reflect, approximately, the total level of Poisson distributed spiking (or spike arrivals) in a local patch of cortex (Miller et al., 2009a). In contrast, the narrowband gamma response is caused by neural activity with a high level of cell-to-cell synchrony (Singer, 1999) and likely depends on specialized circuitry (Buzsaki and Wang, 2012). While the two responses are sometimes distinguished as 'high gamma' (referring to broadband signals), and 'low gamma' (referring to oscillatory signals), this distinction is not general. Broadband signals can extend into low frequencies (Miller et al., 2009b; Winawer et al., 2013) so that the two signals can overlap in frequency bands. Hence separating gamma band field potentials into an oscillatory component and a broadband (non-oscillatory) component is not reliably accomplished by binning the signals into two temporal frequency bands, one low and one high, but rather requires a model-based analysis, such as fitting the spectrum as the sum of a baseline power law (to capture the broadband component) and a log-Gaussian bump (to capture the oscillatory component) (Hermes et al., 2015b).

There is strong experimental support for the idea that increases in broadband LFP power primarily reflect increases in asynchronous neural activity rather than increases in coherence. First, experiments have shown that broadband power is correlated with multiunit spiking activity (Manning et al., 2009; Ray and Maunsell, 2011). Second, unlike the case of narrowband gamma LFP, changes in broadband LFP are not accompanied by changes in broadband spike-field coupling ((Jia et al., 2013a), their Figure 1A-B). The possibility that neuronal synchrony sometimes affects broadband signals cannot be ruled out, for example as shown in cases of pharmacological manipulations in nonhuman primate (Musall et al., 2014). In such cases, there would not be a simple relationship between broadband power and BOLD.

The prior literature has not shown definitively whether broadband LFP, narrowband gamma, or both predict the BOLD signal. The first study that directly compared simultaneously recorded BOLD and electrophysiology showed that both LFP power in the gamma frequency range (40-130 Hz) and multi unit spiking activity (MUA) predicted the BOLD signal (Logothetis et al., 2001), and further, that when the LFP power diverged from MUA, the gamma band LFP predicted the BOLD signal more accurately than did spiking. This study however did not separately test whether a narrowband (oscillatory) or a broadband (non-oscillatory) component of the LFP better predicted the BOLD response.

Other studies, too, have shown a variety of patterns when correlating LFP power changes in the gamma band with BOLD. Some reported that BOLD amplitude correlates with narrowband gamma

activity (Niessing et al., 2005), while others showed that BOLD correlates with broadband changes (Winawer et al., 2013), and many did not distinguish narrowband from broadband power in the gamma band (Engell et al., 2012). Simultaneous recordings of hemodynamic and neuronal activity in macaque V1 showed that BOLD signals from intrinsic optical images can occur in the absence of gamma band LFP changes (Sirotin and Das, 2009), and that in some circumstances, multiunit activity predicts the BOLD signal more accurately than gamma band LFP (Burns et al., 2010; Lima et al., 2014).

Here we separately quantified the broadband power (spanning at least 50-150 Hz) and narrowband gamma power. We found that the amplitude of broadband changes accurately predicted the BOLD signal in V1. The empirical results and the models help resolve the question of why 'high gamma' has been shown to correlate with BOLD, and 'low gamma' sometimes does not (Lima et al., 2014). The likely reason is unrelated to the difference in frequency range, nor to the size of the spectral perturbation in the local field potential. In fact, the elevation broadband power is relatively small (2 or 3 fold) compared to the elevation in power often observed in narrowband gamma oscillations (10 x or more)(Hermes et al., 2015b). Instead "High gamma" is predictive of the BOLD signal in many cases not because of the specific frequency range, but because this signal captures the level of asynchronous neuronal response; this signal happens to be most clearly visible in the high frequency range (>100 Hz) where it is not masked by rhythmic lower frequency responses. Hence the distinction in predicting the BOLD response is not about "high" versus "low" gamma, but rather synchronous versus asynchronous responses, and the broadband signal, sometimes labeled high gamma, maps onto the first term on the right hand side of Equation 4, the portion of the field potential measurement which sums the energy demand of each neuron.

Our model fits and data support this view. When we captured the stimulus-related broadband response by simulating a change in broadband coherence across neurons rather than a change in the level of response in each neuron, our predicted BOLD response was highly inaccurate (Supplementary Figure S7).

3.2 Changes in narrowband gamma power do not predict BOLD

In contrast, we propose that 'low gamma' often does not predict the BOLD response because 'low gamma' reflects narrowband oscillatory processes, which largely arise from a change in neuronal coherence across the population rather than a change in the level of neuronal population activity. This corresponds to the second term in the right hand side of Equation 4, the portion of the field potential measurement which reflects the cross-power arising from currents in different neurons, and which in our model is independent of the signals giving rise to the BOLD signal.

Our results and model do not argue that narrowband gamma oscillations will never be predictive of the BOLD signal. If in a particular experiment narrowband gamma oscillations were to co-vary with broadband increases, we would expect both signals to correlate with BOLD. This might occur in an experiment with gratings of different contrast; with increasing contrast narrowband gamma responses, broadband responses, and BOLD responses all increase (Jia et al., 2013b; Scheeringa et al., 2011) and all 3 measures would correlate across stimuli. In such an experiment, if narrowband gamma oscillations had a higher signal to noise ratio than the broadband response, then the oscillatory signal would likely show a higher correlation with BOLD. In contrast, when the choice of stimulus or task can independently modulate broadband power and gamma oscillations so that the two LFP measures are not correlated, as in the experiments presented here and previously (Hermes et al., 2015b), then gamma oscillations will not strongly correlate with BOLD.

Our simulation and empirical results are consistent with studies which varied chromatic contrast and spatial frequency, while measuring MEG and BOLD. These studies found that BOLD and

narrowband gamma activity did not match in stimulus specificity (Muthukumaraswamy and Singh, 2009; Swettenham et al., 2013). It is likely that these stimulus manipulations, like ours, independently modulated narrowband gamma power and broadband power, although the studies did not quantify broadband fields, which are more challenging to measure with MEG than with ECoG (Dalal et al., 2009). We speculate that broadband fields spanning the gamma range would have shown a higher correlation with BOLD.

3.3 Neuronal synchrony and the BOLD signal

In our model, the LFP measures are highly sensitive to neuronal synchrony, whereas BOLD is not. In our simulations, increases in neuronal synchrony drove narrowband gamma oscillations in the field potential. There are other cases of population activity with a high degree of neuronal synchrony. One example is the steady state evoked potential associated with a periodic stimulus (first reported by Adrian and Matthews, 1934; reviewed by Norcia et al., 2015). Previous studies have described discrepancies between evoked potentials and the BOLD signal, such as in the case of spatial summation (Winawer et al., 2013), directional motion selectivity (Ales and Norcia, 2009; Huk et al., 2001) and spatial attention (Itthipuripat et al., 2014; Pestilli et al., 2011). Our modeling framework suggests that the neural sources generating the steady state potential (synchronous neural activity) are likely to be only weakly related to the BOLD signal (depending largely on asynchronous signals), as these sources will primarily affect the second term on the right hand side of Equation 4 (cross-power). This does not imply that the two measures are always or even usually discrepant; the BOLD signal and steady state potentials are likely to correlate any time that the steady state signals correlate with other measures of neural activity. When measures do dissociate, we do not conclude that one measure is more accurate; instead, the measures offer complementary views of the population activity, emphasizing the degree of synchrony or the average level of the response. An intriguing question is how each of the two signals contributes to perception and behavior.

Neural synchrony can also emerge without being time-locked to the stimulus, often called 'induced synchrony' or 'induced oscillations' (Tallon-Baudry and Bertrand, 1999). In our simulation, we assumed that narrowband gamma LFP changes were induced by increases in *synchrony* between neurons, and not by changes in the *level* of gamma power within the individual neurons. In contrast, we assumed that broadband LFP increases were induced by increased broadband activity in individual neurons, and not by increased broadband coherence between neurons. (In Equation 4, a change in the left hand side, LFP power in the gamma band, can be produced by a change in either the first or second term on the right). This explains why, in our simulation, the broadband power was correlated with BOLD whereas the LFP gamma power was not, findings that were also confirmed by the data. Were our assumptions justified?

In principle, an increase in narrowband gamma power in the LFP could arise because the neurons synchronize in the gamma band, or because ongoing gamma oscillations within each neuron increase in amplitude, independent of coordination between neurons. There is strong experimental support for the former. Experiments which measure both intracellular membrane potential from single neurons and the extracellular LFP show that when there is an increase in narrowband LFP gamma power, the gamma power from individual neurons becomes more coherent with the LFP (Perrenoud et al., 2016). Moreover, the coherence between local spiking and the LFP also increases in the gamma band when LFP gamma power increases (Jia et al., 2013a). These results are consistent with our assumption that a significant part of the increase in gamma LFP power arises from a change in population coherence. To our knowledge, it is not certain whether there is also some increase in the level of gamma signals within individual neurons when the narrowband gamma band LFP power changes. However, since we can attribute a large part of the change in

gamma LFP to a change in coherence, we infer that we can only attribute, at most, a small part of the change in gamma LFP to the level of gamma power within neurons.

In our simulation, we made two simple but extreme assumptions. First, we assumed that gamma oscillations occur with no change in the total level of neural activity, and hence no change in metabolic demand or BOLD. Second, we assumed that broadband responses occur with no change in neural synchrony. While these assumptions are likely incorrect at the limit, the simulations nonetheless captured the pattern of ECoG and fMRI results obtained in our datasets. Alternative models in which the broadband response was caused by a change in synchrony were much less accurate (Supplementary Figure S7). Models in which gamma responses were caused by a change in level were only slightly less accurate, and cannot be ruled out entirely (Supplementary Figure S7). However the regression models fit to our data (Figure 7) show that the power of narrowband gamma oscillations does not predict the BOLD response. Hence the most parsimonious explanation is that these responses in the LFP are caused in large part by changes in synchrony.

3.4 DC offsets and the BOLD signal

Both our measurements and our simulations showed that broadband electrophysiological responses were related to, but did not fully account for, the BOLD signal. This was especially evident in Simulation 2 and extrastriate data (V2/V3). In these cases, the amplitude of low frequency oscillations (8-15 Hz) was negatively correlated with the BOLD signal, independent of broadband signals. Numerous previous studies have reported that low frequency oscillations are anti-correlated with BOLD, including measurements in motor, visual and language areas (Harvey et al., 2013; Hermes et al., 2012; Hermes et al., 2014; Magri et al., 2012; Maier et al., 2008; Scheeringa et al., 2011). This result may appear to conflict with the prior discussion, since we argued that oscillations (to the degree that they reflect neuronal synchrony) should have little to no effect on metabolic demand or the BOLD signal. It is therefore important to ask why low frequency oscillations sometimes correlate with the BOLD signal, both in data and in simulation.

One explanation is that alpha oscillations, or a mechanism which generates the oscillations, affect the BOLD signal indirectly, by inhibiting cortical activity. According to this explanation, an increase in alpha power results in a decrease in local spiking activity in turn reducing metabolic demand and the BOLD signal (Harris and Thiele, 2011). Alpha oscillations may indeed co-occur with reduced cortical excitation (Mazaheri and Jensen, 2010). However, if this coupling between alpha power and spiking were the only explanation for the relationship between alpha power and BOLD, then a more direct measure of neuronal excitation, such as broadband or multiunit activity, would adequately predict the BOLD signal; alpha power would negatively correlate with the BOLD signal, but would provide no *additional* predictive power. Our data and model do not support this explanation, as we find that for most cortical sites, the most accurate predictor of the BOLD signal is a combined model including both the amplitude of alpha oscillations and broadband power.

We therefore propose that in addition to the indirect effect of modulating cortical excitability, alpha oscillations are also accompanied by a DC shift in membrane potential, making it less depolarized (i.e., closer to the equilibrium potential), and this shift reduces metabolic demand. Indirect evidence for a DC shift comes from MEG and ECoG studies (Jensen and Mazaheri, 2010; Mazaheri and Jensen, 2008; Schalk, 2015) and can be explained by a simple process: if alpha oscillations reflect periodic inhibitory pulses, then on average they will cause a depolarization. If the neuron was slightly depolarized before the inhibitory alpha pulses, then the pulses would push the neuron toward equilibrium, and hence a lower energy state. In this view, large alpha oscillations reflect larger inhibitory pulses, and hence reducing depolarization. We suggest that this reduced depolarization affects metabolic demand in two ways: by reducing spiking (as discussed above), and by maintaining a less depolarized state, reducing metabolic demand. In our model, the contribution to

the BOLD signal from each neuron is the power in the time series (Equation 3), and the mean contributes to power. The idea that a DC shift in the membrane potential affects metabolic demand (in addition to altering excitability) is consistent with the observation that slowly changing currents (<0.5 Hz) correlate with BOLD fluctuations (Goense and Logothetis, 2008; Raichle, 2010).

3.5 A single modeling framework accounts for patterns of LFP/BOLD correlations across sites

We found that the relationship between the BOLD signal and features of the ECoG data differed across cortical areas. For example, broadband changes in ECoG responses explained more variance in the BOLD data in V1 than in V2/V3. Conversely, low frequency power decreases (alpha, 8-13Hz) explained more variance in the BOLD signal in V2/V3 than in V1. In the absence of a model, we might have interpreted the results as evidence that neurovascular coupling differs across sites. Many previous studies have reported differences in the relation between LFP and BOLD as a function of site or condition, for example between cortical and subcortical locations (Sloan et al., 2010), across cortical regions (Conner et al., 2011; Huo et al., 2014), between cortical layers (Goense et al., 2012), and as a function of medication (Zaldivar et al., 2014). Here, we showed that a difference in the relationship between LFP and BOLD need not arise because of a difference in neurovascular coupling. In our results, Simulations 1 and 2, like V1 compared to extrastriate areas, showed differences in the relationship between LFP and BOLD, yet we used the identical model of neurovascular coupling in all simulations. The systematic differences in the two simulations arose because of differences in the neuronal population activity, not because of differences in neurovascular coupling. While our results do not exclude the possibility of differences in neurovascular coupling across locations or states they do caution against interpreting differences in the relationship between field potentials and BOLD as evidence for a difference in neurovascular coupling, since they show that a single model can account for a variety of patterns. More generally, the V1 versus V2/V3 discrepancies bolster the argument that one cannot predict the exact relationship between BOLD and field potentials without also specifying the neuronal population activity.

3.6 The role of a simple model in understanding the relation between BOLD and LFP

A complete description of the biophysical processes giving rise to the BOLD signal and the field potential is far beyond the scope of this paper, and is likely premature given the enormous complexity in the nervous system, the vascular system, and the coupling mechanisms between them. Instead, the purpose of our modeling framework was to first begin with a general principle, namely that BOLD and field potentials sum neural activity according to a different sequence of operations; second, to instantiate this principle in simple mathematical rules; third, to combine these rules with a minimal model of neural population activity; and finally, to ask to what extent such a model can account for the patterns in our data. Our model omits many biophysical components, such as compartmentalized neurons, multiple cell types and vessel types, neurotransmitters, the dynamics of blood flow, and so on, and hence it is not a detailed simulation of the nervous system or vascular system. On the other hand, the simplicity of the model facilitates an understanding derived from basic principles, similar to the advantages in building computational, rather than biophysical, models of neural responses (Carandini and Heeger, 2012; Heeger et al., 1996; Kay et al., 2013b; Wandell, 1995). Both types of models and empirical studies are valuable. Here we emphasize that even with a highly simplified model of the BOLD signal, the field potential, and neuronal population activity, we are able to reconcile a wide range of findings in a complicated and technical literature. The model accounts for differences in how broadband field potentials and gamma oscillations relate to the BOLD signal. It can explain differences between cortical areas in the relationship between field potentials and BOLD. The model also provides an

explanation for why the amplitude of alpha rhythms is negatively correlated with BOLD, even after accounting for the relationship between broadband signals and BOLD.

3.7 Reproducible computations

To test competing computational theories about the relation between the visual input, the LFP and the BOLD response, it is essential to make sample data and code available for others (Hermes et al., 2015a; Hermes et al., 2015b). Following standard practices of reproducible research (Axelrod, 2014; Gavish and Donoho, 2012; LeVeque et al., 2012), the Matlab code of the simulation, and sample data and code to reproduce the figures in this manuscript can be downloaded at https://github.com/WinawerLab/BOLD_LFP.

3.8 Conclusions

To understand how the electrophysiology and BOLD responses are related, it is necessary to specify both the manner in which population activity transfers to the two signals, and the neuronal population activity itself. The former shows that the covariance between neuronal time series has a large influence on the field potential and not the BOLD signal. Based on our simulations and empirical results, we made several inferences about the neuronal population responses mediating the BOLD signal and the LFP: that narrowband gamma oscillations in visual cortex likely arise more from synchronization of neural responses than a change in level of the neural response, and hence have a large influence on the field potential and little influence on the BOLD signal; that responses which are asynchronous across neurons manifest in broadband field potentials and an elevated BOLD signal; and that low frequency oscillations observed in field potentials are likely accompanied by a widespread hyperpolarization, which in turn reduces metabolic demand and the BOLD signal. Our model-based approach brings us a step closer to a general solution to the question of how neural activity relates to the BOLD signal.

4. Experimental Procedures

4.1 Simulated neuronal time series

Simulations were computed for a population of 200 neurons. Each simulation trial was 1 second long with millisecond sampling. The time series for each neuron was derived by summing three inputs, each 1 second long, followed by leaky integration with a time scale of 10 ms to simulate temporal integration in the dendrite (Figure 2). Each simulation was fit to ECoG data from one electrode and consisted of 240 trials, 8 repeats of 30 stimulus conditions. A condition in the simulation was defined by the parameter settings for the 3 inputs (Figure 4): C^1 (broadband), C^2 (gamma) and C^3 (alpha). See Supplementary Methods for details. Variations in these three inputs resulted in power changes in the broadband, gamma, and alpha LFP. The inputs were fit to data such the simulated LFP power changes matched the ECoG data power changes for a particular electrode and stimulus.

4.2 Stimuli and task

Stimuli for ECoG experiments were reported previously (Hermes et al., 2015b). In brief, for one subject, the stimuli came from 8 classes of patterns (30 exemplars per class, 20x20°), including high contrast vertical gratings (0.16, 0.33, 0.65, or 1.3 cycles per degree square wave) noise patterns (spectral power distributions of k/f^4, k/f^2, and k/f^0), and a blank screen at mean luminance (Supplementary methods and Supplementary Figure S2). For the second ECoG subject, there were the same 8 classes as well as two other stimulus classes – a high contrast white noise pattern and a plaid at 0.65 cpd. The fMRI subjects had the same 10 stimulus classes as the second ECoG subject.

4.3 ECoG procedure

ECoG data were measured from two subjects who were implanted with subdural electrodes (2.3 mm diameter, AdTech Medical Instrument Corp) for clinical purposes at Stanford Hospital. Informed, written consent was obtained from all subjects. ECoG protocols were approved by the Stanford University IRB. In 22 channels in V1 V2 and V3, broadband and narrowband gamma responses were quantified as before (Hermes et al., 2015b), and alpha power changes were calculated (see Supplementary Methods).

4.4 fMRI procedure

Functional MRI data was measured from four subjects (3 female, ages 22-42) with normal or corrected-to-normal vision at the Center for Brain Imaging at NYU. Informed, written consent was obtained from all subjects. The fMRI protocols were approved by the New York University IRB. Functional MRI data were preprocessed and analyzed using custom software (http://vistalab.stanford.edu/software) (see Supplementary Methods). Disc ROIs (radius = 2 mm) were defined in fMRI subjects to match the position of the electrodes in ECoG subjects using a combination of anatomy, pRF centers, and visual field maps. The similarity between the ROI position and electrode position was compared via visual inspection of anatomical images and pRF centers (Supplementary Figure S3).

4.5 Predicting fMRI signals directly from ECoG models

The relationship between fMRI and ECoG signals was analyzed using a linear regression model. The cross-validated R2 was used as a metric for model quality and the regression coefficients were used to test whether ECoG predictors (broadband, gamma and alpha) had a positive or negative relation with BOLD (also see Supplementary Methods).

Acknowledgements

We thank two colleagues for making important contributions to our analytic framework. David J Heeger (NYU) proposed to us that the two measures, BOLD and LFP, could be approximated by the same operations computed in a different order (captured in Equations 1-3) and Weiji Ma (NYU) derived a variant of Equation 4 for us, expressing analytically the quantitative difference that results from the difference in the order of operations. This work was supported by the National Eye Institute at National Institutes of Health grant R00-EY022116 to J.W. and T32-EY20485 to D.H. The ECoG data, which was previously published and re-analyzed for this paper, was provided as part of the Stanford Human Intracranial Cognitive Epilepsy Program (SHiCEP), headed by Josef Parvizi. We also thank Brian A Wandell, David J, Heeger, Rachel Denison, Noah Benson, and Nathan Witthoft for helpful comments on an earlier draft of the manuscript. The empirical results were presented at VSS in 2015 and the modeling components have been presented at SfN 2015.

References

Adrian, E.D., and Matthews, B.H.C. (1934). The Berger rhythm: Potential changes from the occipital lobes in man. Brain 57, 355-385.
Ales, J.M., and Norcia, A.M. (2009). Assessing direction-specific adaptation using the steady-state visual evoked potential: results from EEG source imaging. J Vis 9, 8.
Axelrod, V. (2014). Minimizing bugs in cognitive neuroscience programming. Frontiers in psychology 5.
Bao, P., Purington, C.J., and Tjan, B.S. (2015). Using an achiasmic human visual system to quantify the relationship between the fMRI BOLD signal and neural response. Elife 4.
Bedard, C., and Destexhe, A. (2009). Macroscopic models of local field potentials and the apparent 1/f noise in brain activity. Biophys J 96, 2589-2603.
Bedard, C., Kroger, H., and Destexhe, A. (2006). Does the 1/f frequency scaling of brain signals reflect self-organized critical states? Phys Rev Lett 97, 118102.
Benson, N.C., Butt, O.H., Datta, R., Radoeva, P.D., Brainard, D.H., and Aguirre, G.K. (2012). The retinotopic organization of striate cortex is well predicted by surface topology. Curr Biol 22, 2081-2085.
Burns, S.P., Xing, D., and Shapley, R.M. (2010). Comparisons of the dynamics of local field potential and multiunit activity signals in macaque visual cortex. J Neurosci 30, 13739-13749.
Burns, S.P., Xing, D., and Shapley, R.M. (2011). Is gamma-band activity in the local field potential of V1 cortex a "clock" or filtered noise? J Neurosci 31, 9658-9664.
Buzsaki, G., Anastassiou, C.A., and Koch, C. (2012). The origin of extracellular fields and currents--EEG, ECoG, LFP and spikes. Nat Rev Neurosci 13, 407-420.
Buzsaki, G., and Wang, X.J. (2012). Mechanisms of gamma oscillations. Annu Rev Neurosci 35, 203-225.
Carandini, M., and Heeger, D.J. (2012). Normalization as a canonical neural computation. Nature reviews Neuroscience 13, 51-62.
Conner, C.R., Ellmore, T.M., Pieters, T.A., DiSano, M.A., and Tandon, N. (2011). Variability of the relationship between electrophysiology and BOLD-fMRI across cortical regions in humans. J Neurosci 31, 12855-12865.
Cottereau, B.R., Ales, J.M., and Norcia, A.M. (2015). How to use fMRI functional localizers to improve EEG/MEG source estimation. Journal of neuroscience methods 250, 64-73.
Dalal, S.S., Baillet, S., Adam, C., Ducorps, A., Schwartz, D., Jerbi, K., Bertrand, O., Garnero, L., Martinerie, J., and Lachaux, J.P. (2009). Simultaneous MEG and intracranial EEG recordings during attentive reading. Neuroimage 45, 1289-1304.
Dumoulin, S.O., and Wandell, B.A. (2008). Population receptive field estimates in human visual cortex. Neuroimage 39, 647-660.
Engell, A.D., Huettel, S., and McCarthy, G. (2012). The fMRI BOLD signal tracks electrophysiological spectral perturbations, not event-related potentials. Neuroimage 59, 2600-2606.
Freeman, J., Ziemba, C.M., Heeger, D.J., Simoncelli, E.P., and Movshon, J.A. (2013). A functional and perceptual signature of the second visual area in primates. Nat Neurosci 16, 974-981.
Gavish, M., and Donoho, D. (2012). Three Dream Applications of Verifiable Computational Results. Computing in Science & Engineering 14, 26-31.
George, J.S., Aine, C.J., Mosher, J.C., Schmidt, D.M., Ranken, D.M., Schlitt, H.A., Wood, C.C., Lewine, J.D., Sanders, J.A., and Belliveau, J.W. (1995). Mapping function in the human brain with magnetoencephalography, anatomical magnetic resonance imaging, and functional magnetic resonance imaging. J Clin Neurophysiol 12, 406-431.

Goense, J., Merkle, H., and Logothetis, N.K. (2012). High-resolution fMRI reveals laminar differences in neurovascular coupling between positive and negative BOLD responses. Neuron 76, 629-639.
Goense, J.B., and Logothetis, N.K. (2008). Neurophysiology of the BOLD fMRI signal in awake monkeys. Curr Biol 18, 631-640.
Gray, C.M., Konig, P., Engel, A.K., and Singer, W. (1989). Oscillatory responses in cat visual cortex exhibit inter-columnar synchronization which reflects global stimulus properties. Nature 338, 334-337.
Gray, C.M., and Singer, W. (1989). Stimulus-specific neuronal oscillations in orientation columns of cat visual cortex. Proceedings of the National Academy of Sciences of the United States of America 86, 1698-1702.
Hämäläinen, M., Hari, R., Ilmoniemi, R.J., Knuutila, J., and Lounasmaa, O.V. (1993). Magnetoencephalography—theory, instrumentation, and applications to noninvasive studies of the working human brain. Reviews of modern Physics 65, 413.
Harris, K.D., and Thiele, A. (2011). Cortical state and attention. Nature reviews Neuroscience 12, 509-523.
Harvey, B.M., Vansteensel, M.J., Ferrier, C.H., Petridou, N., Zuiderbaan, W., Aarnoutse, E.J., Bleichner, M.G., Dijkerman, H.C., van Zandvoort, M.J., Leijten, F.S.*, et al.* (2013). Frequency specific spatial interactions in human electrocorticography: V1 alpha oscillations reflect surround suppression. Neuroimage 65, 424-432.
Hasenstaub, A., Shu, Y., Haider, B., Kraushaar, U., Duque, A., and McCormick, D.A. (2005). Inhibitory postsynaptic potentials carry synchronized frequency information in active cortical networks. Neuron 47, 423-435.
Heeger, D.J., Huk, A.C., Geisler, W.S., and Albrecht, D.G. (2000). Spikes versus BOLD: what does neuroimaging tell us about neuronal activity? Nat Neurosci 3, 631-633.
Heeger, D.J., and Ress, D. (2002). What does fMRI tell us about neuronal activity? Nature reviews Neuroscience 3, 142-151.
Heeger, D.J., Simoncelli, E.P., and Movshon, J.A. (1996). Computational models of cortical visual processing. Proc Natl Acad Sci U S A 93, 623-627.
Henrie, J.A., and Shapley, R. (2005). LFP power spectra in V1 cortex: the graded effect of stimulus contrast. Journal of neurophysiology 94, 479-490.
Hermes, D., Miller, K.J., Noordmans, H.J., Vansteensel, M.J., and Ramsey, N.F. (2010). Automated electrocorticographic electrode localization on individually rendered brain surfaces. Journal of neuroscience methods 185, 293-298.
Hermes, D., Miller, K.J., Vansteensel, M.J., Aarnoutse, E.J., Leijten, F.S., and Ramsey, N.F. (2012). Neurophysiologic correlates of fMRI in human motor cortex. Human brain mapping 33, 1689-1699.
Hermes, D., Miller, K.J., Vansteensel, M.J., Edwards, E., Ferrier, C.H., Bleichner, M.G., van Rijen, P.C., Aarnoutse, E.J., and Ramsey, N.F. (2014). Cortical theta wanes for language. Neuroimage 85 Pt 2, 738-748.
Hermes, D., Miller, K.J., Wandell, B.A., and Winawer, J. (2015a). Gamma oscillations in visual cortex: the stimulus matters. Trends Cogn Sci 19, 57-58.
Hermes, D., Rangarajan, V., Foster, B.L., King, J.R., Kasikci, I., Miller, K.J., and Parvizi, J. (2015b). Electrophysiological Responses in the Ventral Temporal Cortex During Reading of Numerals and Calculation. Cereb Cortex.
Huk, A.C., Ress, D., and Heeger, D.J. (2001). Neuronal basis of the motion aftereffect reconsidered. Neuron 32, 161-172.
Huo, B.X., Smith, J.B., and Drew, P.J. (2014). Neurovascular coupling and decoupling in the cortex during voluntary locomotion. J Neurosci 34, 10975-10981.
Itthipuripat, S., Ester, E.F., Deering, S., and Serences, J.T. (2014). Sensory gain outperforms efficient readout mechanisms in predicting attention-related improvements in behavior. J Neurosci 34, 13384-13398.

Jensen, O., and Mazaheri, A. (2010). Shaping functional architecture by oscillatory alpha activity: gating by inhibition. Front Hum Neurosci 4, 186.
Jia, X., Smith, M.A., and Kohn, A. (2011). Stimulus selectivity and spatial coherence of gamma components of the local field potential. J Neurosci 31, 9390-9403.
Jia, X., Tanabe, S., and Kohn, A. (2013a). gamma and the coordination of spiking activity in early visual cortex. Neuron 77, 762-774.
Jia, X., Xing, D., and Kohn, A. (2013b). No consistent relationship between gamma power and peak frequency in macaque primary visual cortex. J Neurosci 33, 17-25.
Kay, K.N., Rokem, A., Winawer, J., Dougherty, R.F., and Wandell, B.A. (2013a). GLMdenoise: a fast, automated technique for denoising task-based fMRI data. Frontiers in neuroscience 7, 247.
Kay, K.N., Winawer, J., Rokem, A., Mezer, A., and Wandell, B.A. (2013b). A two-stage cascade model of BOLD responses in human visual cortex. PLoS Comput Biol 9, e1003079.
Kay, K.N., Winawer, J., Rokem, A., Mezer, A., and Wandell, B.A. (2013c). A two-stage cascade model of BOLD responses in human visual cortex. PLoS Comput Biol 9, e1003079.
Koch, C., Rapp, M., and Segev, I. (1996). A brief history of time (constants). Cereb Cortex 6, 93-101.
Lachaux, J.P., Fonlupt, P., Kahane, P., Minotti, L., Hoffmann, D., Bertrand, O., and Baciu, M. (2007). Relationship between task-related gamma oscillations and BOLD signal: new insights from combined fMRI and intracranial EEG. Hum Brain Mapp 28, 1368-1375.
Lee, J.H., Durand, R., Gradinaru, V., Zhang, F., Goshen, I., Kim, D.S., Fenno, L.E., Ramakrishnan, C., and Deisseroth, K. (2010). Global and local fMRI signals driven by neurons defined optogenetically by type and wiring. Nature 465, 788-792.
LeVeque, R.J., Mitchell, I.M., and Stodden, V. (2012). Reproducible Research for Scientific Computing: Tools and Strategies for Changing the Culture. Computing in Science & Engineering 14, 13-17.
Lima, B., Cardoso, M.M., Sirotin, Y.B., and Das, A. (2014). Stimulus-related neuroimaging in task-engaged subjects is best predicted by concurrent spiking. J Neurosci 34, 13878-13891.
Llinas, R.R., Grace, A.A., and Yarom, Y. (1991). In vitro neurons in mammalian cortical layer 4 exhibit intrinsic oscillatory activity in the 10- to 50-Hz frequency range. Proc Natl Acad Sci U S A 88, 897-901.
Logothetis, N.K., Kayser, C., and Oeltermann, A. (2007). In vivo measurement of cortical impedance spectrum in monkeys: implications for signal propagation. Neuron 55, 809-823.
Logothetis, N.K., Pauls, J., Augath, M., Trinath, T., and Oeltermann, A. (2001). Neurophysiological investigation of the basis of the fMRI signal. Nature 412, 150-157.
Logothetis, N.K., and Wandell, B.A. (2004). Interpreting the BOLD signal. Annu Rev Physiol 66, 735-769.
Magri, C., Schridde, U., Murayama, Y., Panzeri, S., and Logothetis, N.K. (2012). The amplitude and timing of the BOLD signal reflects the relationship between local field potential power at different frequencies. J Neurosci 32, 1395-1407.
Maier, A., Wilke, M., Aura, C., Zhu, C., Ye, F.Q., and Leopold, D.A. (2008). Divergence of fMRI and neural signals in V1 during perceptual suppression in the awake monkey. Nat Neurosci 11, 1193-1200.
Manning, J.R., Jacobs, J., Fried, I., and Kahana, M.J. (2009). Broadband shifts in local field potential power spectra are correlated with single-neuron spiking in humans. J Neurosci 29, 13613-13620.
Mathiesen, C., Caesar, K., Akgoren, N., and Lauritzen, M. (1998). Modification of activity-dependent increases of cerebral blood flow by excitatory synaptic activity and spikes in rat cerebellar cortex. J Physiol 512 (Pt 2), 555-566.
Mazaheri, A., and Jensen, O. (2008). Asymmetric amplitude modulations of brain oscillations generate slow evoked responses. J Neurosci 28, 7781-7787.
Mazaheri, A., and Jensen, O. (2010). Rhythmic pulsing: linking ongoing brain activity with evoked responses. Front Hum Neurosci 4, 177.

Miller, K.J., Sorensen, L.B., Ojemann, J.G., and den Nijs, M. (2009a). Power-law scaling in the brain surface electric potential. PLoS Comput Biol 5, e1000609.
Miller, K.J., Zanos, S., Fetz, E.E., den Nijs, M., and Ojemann, J.G. (2009b). Decoupling the cortical power spectrum reveals real-time representation of individual finger movements in humans. J Neurosci 29, 3132-3137.
Milstein, J., Mormann, F., Fried, I., and Koch, C. (2009). Neuronal shot noise and Brownian 1/f2 behavior in the local field potential. PloS one 4, e4338.
Mukamel, R., Gelbard, H., Arieli, A., Hasson, U., Fried, I., and Malach, R. (2005). Coupling between neuronal firing, field potentials, and FMRI in human auditory cortex. Science 309, 951-954.
Musall, S., von Pfostl, V., Rauch, A., Logothetis, N.K., and Whittingstall, K. (2014). Effects of neural synchrony on surface EEG. Cereb Cortex 24, 1045-1053.
Muthukumaraswamy, S.D., and Singh, K.D. (2009). Functional decoupling of BOLD and gamma-band amplitudes in human primary visual cortex. Hum Brain Mapp 30, 2000-2007.
Niessing, J., Ebisch, B., Schmidt, K.E., Niessing, M., Singer, W., and Galuske, R.A. (2005). Hemodynamic signals correlate tightly with synchronized gamma oscillations. Science 309, 948-951.
Norcia, A.M., Appelbaum, L.G., Ales, J.M., Cottereau, B.R., and Rossion, B. (2015). The steady-state visual evoked potential in vision research: A review. J Vis 15, 4.
Ojemann, G.A., Ojemann, J., and Ramsey, N.F. (2013). Relation between functional magnetic resonance imaging (fMRI) and single neuron, local field potential (LFP) and electrocorticography (ECoG) activity in human cortex. Front Hum Neurosci 7, 34.
Perrenoud, Q., Pennartz, C.M., and Gentet, L.J. (2016). Membrane Potential Dynamics of Spontaneous and Visually Evoked Gamma Activity in V1 of Awake Mice. PLoS Biol 14, e1002383.
Pesaran, B. (2008). Spectral analysis for neural signals. In Neural Signal Processing: Quantitative Analysis of Neural Activity, P. Mitra, ed. (Society for Neuroscience), pp. 1-12.
Pestilli, F., Carrasco, M., Heeger, D.J., and Gardner, J.L. (2011). Attentional enhancement via selection and pooling of early sensory responses in human visual cortex. Neuron 72, 832-846.
Pfurtscheller, G., Stancak, A., Jr., and Neuper, C. (1996). Event-related synchronization (ERS) in the alpha band--an electrophysiological correlate of cortical idling: a review. Int J Psychophysiol 24, 39-46.
Raichle, M.E. (2010). Two views of brain function. Trends in cognitive sciences 14, 180-190.
Raichle, M.E., and Mintun, M.A. (2006). Brain work and brain imaging. Annu Rev Neurosci 29, 449-476.
Ray, S., and Maunsell, J.H. (2011). Different origins of gamma rhythm and high-gamma activity in macaque visual cortex. PLoS Biol 9, e1000610.
Rees, G., Friston, K., and Koch, C. (2000). A direct quantitative relationship between the functional properties of human and macaque V5. Nat Neurosci 3, 716-723.
Schalk, G. (2015). A general framework for dynamic cortical function: the function-through-biased-oscillations (FBO) hypothesis. Front Hum Neurosci 9, 352.
Scheeringa, R., Fries, P., Petersson, K.M., Oostenveld, R., Grothe, I., Norris, D.G., Hagoort, P., and Bastiaansen, M.C. (2011). Neuronal dynamics underlying high- and low-frequency EEG oscillations contribute independently to the human BOLD signal. Neuron 69, 572-583.
Scheeringa, R., Koopmans, P.J., van Mourik, T., Jensen, O., and Norris, D.G. (2016). The relationship between oscillatory EEG activity and the laminar-specific BOLD signal. Proc Natl Acad Sci U S A.
Shmuel, A., Augath, M., Oeltermann, A., and Logothetis, N.K. (2006). Negative functional MRI response correlates with decreases in neuronal activity in monkey visual area V1. Nature neuroscience 9, 569-577.
Singer, W. (1999). Neuronal synchrony: a versatile code for the definition of relations? Neuron 24, 49-65, 111-125.

Sirotin, Y.B., and Das, A. (2009). Anticipatory haemodynamic signals in sensory cortex not predicted by local neuronal activity. Nature 457, 475-479.
Sloan, H.L., Austin, V.C., Blamire, A.M., Schnupp, J.W., Lowe, A.S., Allers, K.A., Matthews, P.M., and Sibson, N.R. (2010). Regional differences in neurovascular coupling in rat brain as determined by fMRI and electrophysiology. Neuroimage 53, 399-411.
Smith, A.M., Lewis, B.K., Ruttimann, U.E., Ye, F.Q., Sinnwell, T.M., Yang, Y., Duyn, J.H., and Frank, J.A. (1999). Investigation of low frequency drift in fMRI signal. Neuroimage 9, 526-533.
Swettenham, J.B., Muthukumaraswamy, S.D., and Singh, K.D. (2013). BOLD Responses in Human Primary Visual Cortex are Insensitive to Substantial Changes in Neural Activity. Front Hum Neurosci 7, 76.
Tallon-Baudry, C., and Bertrand, O. (1999). Oscillatory gamma activity in humans and its role in object representation. Trends Cogn Sci 3, 151-162.
Tan, A.Y., Chen, Y., Scholl, B., Seidemann, E., and Priebe, N.J. (2014). Sensory stimulation shifts visual cortex from synchronous to asynchronous states. Nature 509, 226-229.
Wandell, B.A. (1995). Foundations of vision (Sunderland, Mass.: Sinauer Associates).
Welch, P.D. (1967). Use of Fast Fourier Transform for Estimation of Power Spectra - a Method Based on Time Averaging over Short Modified Periodograms. Ieee T Acoust Speech Au15, 70-&.
Winawer, J., Horiguchi, H., Sayres, R.A., Amano, K., and Wandell, B.A. (2010). Mapping hV4 and ventral occipital cortex: the venous eclipse. J Vis 10, 1.
Winawer, J., Kay, K.N., Foster, B.L., Rauschecker, A.M., Parvizi, J., and Wandell, B.A. (2013). Asynchronous broadband signals are the principal source of the BOLD response in human visual cortex. Curr Biol 23, 1145-1153.
Zaldivar, D., Rauch, A., Whittingstall, K., Logothetis, N.K., and Goense, J. (2014). Dopamine-induced dissociation of BOLD and neural activity in macaque visual cortex. Curr Biol 24, 2805-2811.
Zanos, T.P., Mineault, P.J., and Pack, C.C. (2011). Removal of spurious correlations between spikes and local field potentials. J Neurophysiol 105, 474-486.